



The Effect of Light Penetration Depth on the LCST Phase Behavior of a Thermo- and Photoresponsive Statistical Copolymer in an Ionic Liquid

Cecilia C. Hall ,¹ Cecelia A. Rivera,² Timothy P. Lodge ^{1,2}

¹Department of Chemistry, University of Minnesota, Minneapolis, Minnesota, 55455

²Department of Chemical Engineering and Materials Science, University of Minnesota, Minneapolis, Minnesota, 55455

Correspondence to: T.P. Lodge (E-mail: lodge@umn.edu)

Received 28 March 2018; accepted 16 May 2018; published online 00 Month 2018

DOI: 10.1002/pola.29075

ABSTRACT: A reflection cloud point technique allows for rapid screening of light-dependent phase separation temperatures of thermo- and photoresponsive polymer/ionic liquid solutions as a function of sample thickness, molecular weight, and copolymer composition. We systematically investigate the lower critical solution temperature (LCST) phase behavior of poly(benzyl methacrylate-*stat*-(4-phenylazophenyl methacrylate)). Under UV light, the photoresponsive azobenzene-based repeat unit becomes more polar as the *cis* form dominates, increasing its solubility in the ionic liquids 1-ethyl-3-methyl imidazolium and 1-butyl-3-methyl imidazolium bis(trifluoromethanesulfonyl)imide. This light-dependent polarity change leads to two phase separation temperatures, depending on the illumination wavelength. Under visible light, which drives the azobenzene moiety into the *trans* ground state, the LCST shows no sample thickness

dependence. Under UV light, however, sample thickness plays a significant role. Samples of around 1 mm thickness show no apparent difference under UV and visible light, whereas thinner samples show an increasing difference between the phase separation temperatures with decreasing sample thickness. Neither phase separation temperature exhibits a significant dependence on molecular weight. Increasing the photoresponsive monomer content did not lead to an increase in the difference between the phase separation temperatures at fixed thickness, due to a concomitant increase in UV light absorbed at the sample surface. © 2018 Wiley Periodicals, Inc. *J. Polym. Sci., Part A: Polym. Chem.* **2018**, *00*, 000–000

KEYWORDS: azobenzene; ionic liquid; photoresponsive; poly(benzyl methacrylate); stimuli-responsive

INTRODUCTION Appropriate combinations of polymers and ionic liquids yield materials with the desirable properties of the ionic liquid and the mechanical robustness of polymers.^{1,2} The high thermal stability, wide electrochemical windows, high conductivity, and negligible vapor pressures make ionic liquids an attractive choice as solvents for a variety of applications.³ Immobilizing the ionic liquid with polymers gives a wide range of possible applications including electrochemical mechanical actuators,⁴ gate dielectrics in field effect transistors,⁵ gas separation membranes,^{6,7} and fuel cell membranes.⁸ Using stimuli-responsive polymers adds another dimension to the control over the structure of the material, allowing for reversible gel formation or the controlled motion of an actuator.¹⁰ Thermoresponsive polymers have been well-studied in ionic liquids, such as poly(*N*-isopropyl acrylamide) (PNIPAm)^{11,12} and poly(benzyl methacrylate) (PBzMA).^{13–15} PNIPAm in ionic liquids undergoes phase separation on cooling, that is, upper critical solution temperature (UCST) phase behavior. PBzMA in ionic liquids phase separates on heating, following lower critical solution

temperature phase behavior (LCST). Fundamental studies elucidating the phase separation behavior of these polymers enables their extension to applications such as thermoreversible physically associated gels, where the stimuli-responsive polymer is the endblock of an ABA triblock copolymer, with the B block being soluble in the ionic liquid.^{9,16}

Changing temperature to induce phase separation has been well-studied, but this limits potential applications because the system is being physically altered. Controlling the phase separation in a manner that does not physically or chemically alter the system could open up a new range of applications for responsive ionic liquid/polymer systems, such as self-healing materials.^{17–19} Using light as a stimulus could enable such contactless transitions. Azobenzene is a very common light-responsive molecule, where the wavelength of light and temperature control the polarity of the azobenzene, shown in Figure 1.²⁰

The *trans* ground state under visible light is relatively nonpolar, but upon irradiation with UV light the azobenzene unit

Additional Supporting Information may be found in the online version of this article.

© 2018 Wiley Periodicals, Inc.

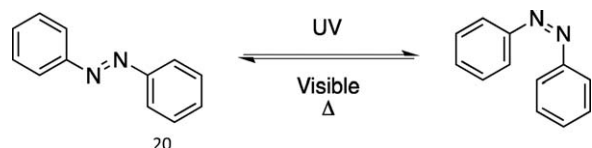


FIGURE 1 *cis/trans* isomerization of azobenzene as a function of light and temperature.

undergoes *trans* to *cis* isomerization, inducing a significant dipole moment.²⁰ It returns to the *trans* ground state via irradiation with visible light, or through thermal relaxation. This change in polarity can be used to change the solubility of a polymer chain in solvent when the azobenzene moiety is incorporated in a monomer.^{19,21–25} 4-Phenylazophenyl methacrylate can be copolymerized with thermoresponsive monomers, where the change in polarity of the azobenzene pendant changes the phase separation temperature. Ideally, the photoresponsive monomer should be a minority component, randomly distributed among the majority thermoresponsive monomer. Photoresponsive phase separation has been well-studied in NIPAm and 4-phenylazophenyl methacrylate (AzoMA) copolymers in ionic liquids, over a range of both copolymer compositions and concentrations. Figure 2 shows the two thermo- and photoresponsive copolymers that will be discussed.

For PNIPAm in ionic liquid, the phase separation temperature is affected by the molecular weight of the polymer¹²; this effect is carried over to PNIPAm/AzoMA copolymers. By incorporating 29 mol% AzoMA in the copolymer, differences in phase separation temperatures under UV and visible light of up to 43 °C were observed.²² In comparison, using 8 mol% AzoMA produced a window of only 8 °C. This difference in phase separation temperatures gives a bistable temperature window, where phase separation can be triggered by light at any intermediate temperature. This approach has been extended to AB diblock copolymers, showing light-induced micellization and de-micellization,²³ as well as to light-induced gelation and gel melting in ABA triblock copolymers.¹⁹ While this system has been demonstrated to be effective, the reactivity ratios of the two monomers are fairly dissimilar. This leads to long reaction times, as both monomers prefer to add AzoMA, which is loaded in small quantities.

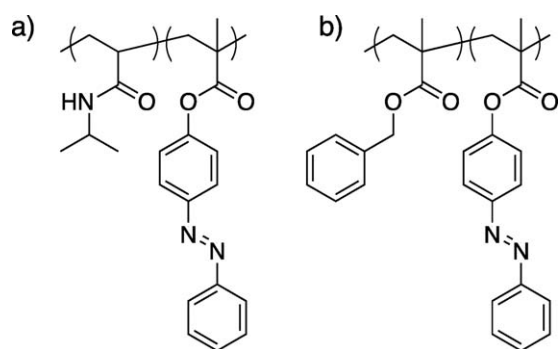


FIGURE 2 Statistical copolymers of (a) NIPAm and AzoMA and (b) BzMA and AzoMA.

Consequently, the AzoMA is not evenly distributed through the chain, which was implicated in the observed broadening of the phase transition for higher AzoMA loadings.

There have also been some studies on BzMA/AzoMA copolymers, focusing on a small range of copolymer compositions, at or below 4 mol% AzoMA incorporation, and low concentrations,²⁴ or as a gel.²⁵ Adding even a small amount of AzoMA depresses the phase separation temperature significantly—PAzoMA homopolymers are insoluble in common ionic liquids. For example, a 28 kDa PBzMA at 3 wt% in 1-ethyl-3-methyl imidazolium bis(trifluoromethanesulfonyl)imide (EMI TFSI) undergoes phase separation at 105 °C.¹⁴ For a 3 wt% solution of a BzMA/AzoMA copolymer with 4 mol% AzoMA incorporation reduced the phase separation temperature under visible light to 80 °C.²⁴ The more polar *cis* isomer increases the solubility of the polymer in the polar ionic liquid, bringing the phase separation temperature up to 102 °C.

For this work, BzMA/AzoMA copolymers are examined in more detail, exploring the phase separation temperature as a function of molecular weight, copolymer composition, and especially sample thickness. These monomers are chemically similar, leading to reactivity ratios that are close to 1 (Supporting Information, Fig. S1). Thus, the monomers are distributed more evenly, making it less likely that the phase transition will broaden with increasing AzoMA content. This allows for investigation of a large range of copolymer compositions, to examine whether the phase transition temperature window increases with increasing AzoMA content in this system. The absolute temperature of the phase transition may change with molecular weight, as is the case with PNIPAm in ionic liquid.¹¹ Finally, sample thickness is a consideration for photoresponsive compounds. The strong absorbance of light drives the isomerization, but it can lead to inhomogeneity in light exposure.²⁶ If the sample is too thick, the light is only able to penetrate a short depth into the sample before it is entirely absorbed. Previous studies of both PNIPAm/AzoMA and BzMA/AzoMA copolymers focused on testing a single sample thickness of 200 μm.^{22,24} Understanding the sample thickness dependence on the phase separation behavior is crucial for extending these polymers to any potential applications. For each polymer examined here, a range of sample thicknesses was measured to investigate how significantly the absorption of the azobenzene chromophore impacts the measured phase transition temperature.

EXPERIMENTAL

Materials

4-Phenylazophenyl methacrylate (AzoMA) was synthesized from methacryloyl chloride and 4-phenylazophenol, as described previously.²⁷ Benzyl methacrylate was purchased from Sigma Aldrich and purified over neutral alumina. 1,1,4,7,10,10-Hexamethyltriethylenetetramine (HMTETA), ethyl α -bromoisobutyrate (EBriB), and anhydrous anisole were used as purchased from Sigma Aldrich. 1-Ethyl-3-methyl

TABLE 1 Molecular Characteristics of P(BzMA-*stat*-AzoMA) Statistical Copolymers

Polymer ^a	mol% incorporation of AzoMA ^b	M_n (kDa) ^c	\bar{D} ^c	Average AzoMA Monomers per Chain ^d
BsA (17-6)	6	17	1.05	5
BsA (35-6)	6	35	1.06	10
BsA (86-6)	6	86	1.09	24
BsA (28-17)	17	28	1.10	24

^a The numbers in parentheses represent the number average molecular weight in kDa and the mol% incorporation of AzoMA, respectively.

^b The incorporation of AzoMA was determined using ¹H NMR spectroscopy.

^c The number average degrees of polymerization and dispersities were determined by SEC.

^d The average AzoMA molecules per chain were determined using the number average molecular weight from SEC and the mol% incorporation of AzoMA from NMR spectroscopy.

imidazolium bromide and 1-butyl-3-methyl imidazolium chloride were used as purchased from Iolitec. Lithium bis(trifluoromethanesulfonyl)imide was used as purchased from 3M. Copper (I) bromide was used as purchased from Riedel-de-Haën. Stainless-steel washers were purchased from McMaster-Carr.

Synthesis of EMI TFSI and BMI TFSI

The ionic liquids were prepared by an ion exchange reaction. The ethyl methyl imidazolium bromide salt (EMI Br, 0.5 mol) or butyl methyl imidazolium bromide salt (BMI Br, 0.5 mol) was mixed with lithium bis(trifluoromethanesulfonyl)imide (Li TFSI, 0.5 mol) in 250 mL of water, then stirred at 70 °C for 48 h. Dichloromethane was added to the reaction, and the water was extracted. The organic layer was washed with deionized H₂O until there was no excess salt present in the water, as determined by a silver nitrate test.

The dichloromethane/ionic liquid mixture was transferred to a round bottom flask and stirred with activated charcoal for 24 h to remove any residual color. After 24 h, the activated charcoal was removed by filtering over neutral alumina, and the dichloromethane was removed via rotary evaporation. The final ionic liquid was dried in a vacuum oven at 70 °C for 72 h. The resulting ionic liquids were characterized by ¹H and ¹⁹F NMR spectroscopy, as shown in Supporting Information, Figures S2 and S3.

Synthesis of P(BzMA-*Stat*-AzoMA)

Copolymers were synthesized using atom transfer radical polymerization (ATRP). In a representative synthesis, benzyl methacrylate (170 mmol), AzoMA (9.0 mmol), HMTETA (0.78 mmol), and EBr*i*B (0.78 mmol) were combined with anisole (90 mL) in a Schlenk flask. The mixture was degassed through three freeze-pump-thaw cycles, then placed under positive pressure of argon. The septum was removed from the reaction flask under a flow of argon, and copper (I) bromide (0.39 mmol) was added. After resealing the flask under argon, the reaction was allowed to proceed at 75 °C for 4 h. The reaction mixture was quenched by placing it in an ice water bath and purified by precipitation in hexanes three times. The resulting polymers were characterized using ¹H NMR spectroscopy (Supporting Information, Fig.

S4) and size-exclusion chromatography (SEC); their properties are summarized in Table 1.

Measurements

Proton nuclear magnetic resonance (¹H NMR) spectra of the polymers were collected using a 500 MHz Bruker Avance II spectrometer, with deuterated chloroform as a solvent. The molecular weight distributions were analyzed using size exclusion chromatography (SEC) paired with refractive index and light scattering detectors, with tetrahydrofuran (THF) as the eluent. The refractive index increment of PAzoMA was measured using an Abbé refractometer (Supporting Information, Fig. S5). UV-vis spectra of the polymers were obtained using a Varian Cary 100 Bio UV-vis spectrophotometer with temperature control (Fig. 5 and Supporting Information, Fig. S6). The UV lamp used was a handheld UVP light source filtered to 365 nm, with a power of 10 mW/cm². The visible light source was a Thor Labs LED with a peak wavelength of 420 nm.

Ionic Liquid Solution Preparation

All polymer/ionic liquid solutions were prepared using the cosolvent method. Polymer and ionic liquid were combined at the desired concentrations to achieve an overall mass of 5 g. THF was added to achieve full dissolution of both polymer and ionic liquid, and the resulting solution was stirred overnight. The THF was removed by purging with nitrogen, and residual solvent was removed by drying in a vacuum oven at room temperature for 72 h.

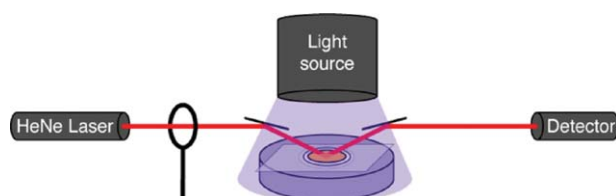


FIGURE 3 Schematic of the thin-film cloud point experimental setup. Laser exposure to the sample is controlled via a shutter between the laser and the sample. The laser is transmitted through the sample using mirrors. The temperature is controlled by placing the sample on a heated, polished aluminum plate. [Color figure can be viewed at wileyonlinelibrary.com]

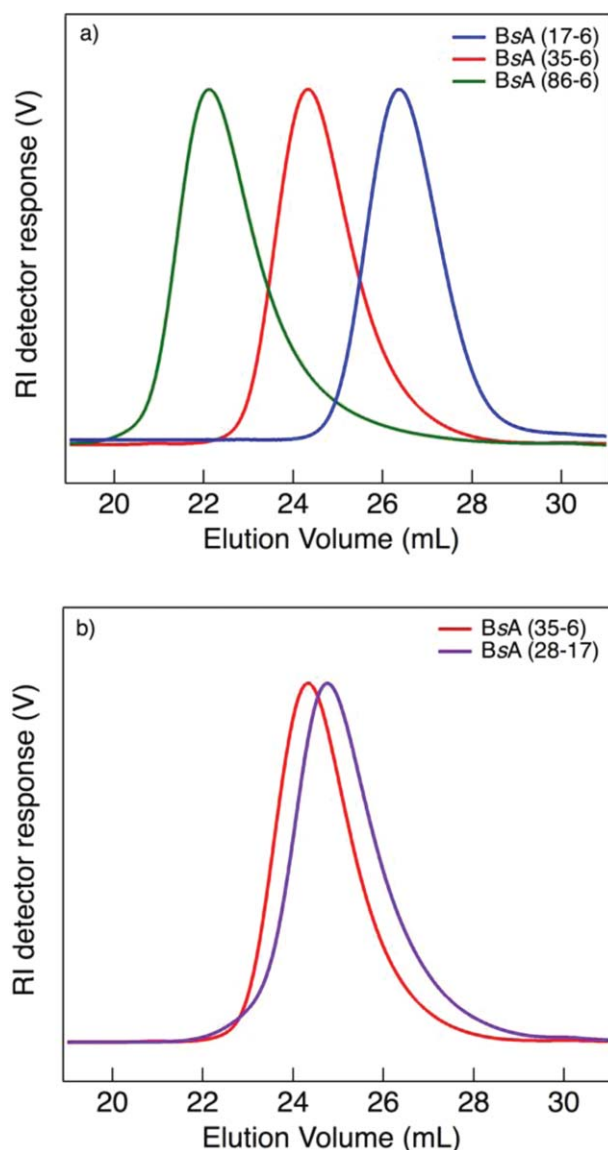


FIGURE 4 SEC traces of P(BzMA-*stat*-AzoMA) with (a) varying molecular weights and 6 mol% AzoMA incorporation, and (b) similar molecular weights and varying AzoMA incorporation. [Color figure can be viewed at wileyonlinelibrary.com]

Cloud Points

The cloud point of each polymer solution was measured in reflection on a home-built instrument, shown in Figure 3. The samples were pipetted onto a microscope slide in the center of a stainless steel washer of a given thickness. A glass coverslip was placed over the sample, and the slides were sealed with epoxy. A HeNe laser ($\lambda = 633$ nm) was reflected down onto the sample using a mirror. When the sample is transparent, the laser is transmitted through the sample and reflected from a polished aluminum plate up to another mirror, which directs the laser toward the detector.

When the sample undergoes phase separation, the transmittance of the laser beam drops as the sample becomes turbid. The desired illumination source was placed directly above the

sample. For visible light measurements, the samples were exposed for 10 min at room temperature, and the experiments were performed in the dark. For UV light measurements, the samples were exposed to the light for 1 h at room temperature, and the UV light remained on for the experiment. The samples reach the steady state of *cis* isomer, shown in Figure 5 and Supporting Information, Figure S6, after 6–7 min. An hour ensures that the higher concentration samples are in the steady state—longer irradiation times did not have an effect on the cloud point. Similarly, a higher UV power of 20 mW/cm² did not affect the cloud point. The samples were heated on the polished aluminum plate using heating cartridges at a rate of 1 °C/min. The temperature was recorded from a thermocouple secured to the top of the microscope slide, to ensure that the temperature reading is as close to sample temperature as possible. A motorized shutter controlled with an Arduino microcontroller reduces the exposure time of the laser on the sample, blocking the beam for 30 s then allowing for transmittance for 10 s. The cloud point is chosen as the point where transmittance is 80% of the maximum value achieved.

RESULTS AND DISCUSSION

To study the effect of molecular weight on the phase separation behavior, the chosen polymers should have narrow molecular weight distributions, with a significant range of average molecular weights. Three polymers of varying molecular weight with a targeted AzoMA incorporation of 5 mol% were synthesized. The actual incorporation of AzoMA obtained was slightly higher, at 6 mol%, due to the reactivity ratios of the two monomers (Supporting Information, Fig. S1). The SEC traces of the three polymers containing 6 mol% AzoMA and varying molecular weights are shown in Figure 4(a). Each polymer shows a single, narrow peak, and the number average molecular weights vary by a factor of five. As well as investigating the impact of molecular weight, it is interesting to consider how changing comonomer composition will affect the phase separation behavior. Accordingly, a fourth polymer was synthesized with a similar molecular weight to BsA (35-6) with the AzoMA incorporation approximately tripled to 17%; the SEC trace is shown in Figure 4(b).

The four polymers were prepared as 10 wt% solutions in ionic liquids. Concentrations below the overlap concentration of the polymer, *ca.* 5 wt% for BsA (35-6), were too dilute to reliably detect a cloud point in the thin film geometry. The cloud point of 28 kDa PBzMA as a 3 wt% solution in EMI TFSI is *ca.* 105 °C,¹⁴ whereas PAzoMA is completely insoluble in both EMI TFSI and BMI TFSI. All BsA polymers with 6 mol% AzoMA were soluble in EMI TFSI at room temperature, with phase separation temperatures in the range of the experimental limits of the home-built cloud point setup. BMI TFSI was used for BsA (28-17), as it was insoluble in EMI TFSI at room temperature.

For each of the four polymer solutions, the cloud points were measured across a range of sample thicknesses. The absorbance of UV light in the AzoMA monomer enables the *trans* to *cis* isomerization that changes the solubility of the

polymer in ionic liquid, but it also means that the UV light has a finite penetration depth through the sample. Figure 5 shows the UV-vis spectrum for 0.02 wt% BsA (28-17) in BMI TFSI. The *trans* isomer has a strong absorbance in the UV region, even at a low concentration and a path length of 2 mm. With this strong absorbance, it was of interest to determine how sample thickness affects the observed phase separation temperature, which required the use of reflective cloud point measurements.

The reflection geometry used for these cloud point measurements was designed to have the laser reflect from a polished aluminum plate when the sample is homogeneously mixed. However, there are also reflections that can occur at the various interfaces (glass-air, coverslip-sample) that can give rise to a measured laser power even when the sample is turbid. As a result, the samples typically never reach 0% transmittance after phase separation occurred. A representative cloud point for BsA (35-6) is shown in Figure 6, where the transmittance shows a clear drop, indicating the cloud point. The cloud point temperature is taken as 80% transmittance scaled to the initial and final transmittance values. As previously demonstrated,²⁴ the *cis* isomer increases the solubility of the polymer under UV light, giving a cloud point ~ 15 °C higher than under visible light.

Each polymer was measured across a range of sample thicknesses from 25 to 1500 μm . The data for the three polymers with 6 mol% AzoMA incorporation are shown in Figure 7(a). The values for all measured cloud points are listed in Supporting Information, Table S1. The cloud point under visible light, shown in open symbols, is independent of sample thickness. Under these conditions the sample is in the *trans* ground state; the 420 nm LED serves to drive any *cis* isomers formed from ambient UV light back to the ground state. There is no significant dependence on molecular weight for the cloud points under visible light. The UV light cloud points, in contrast, show

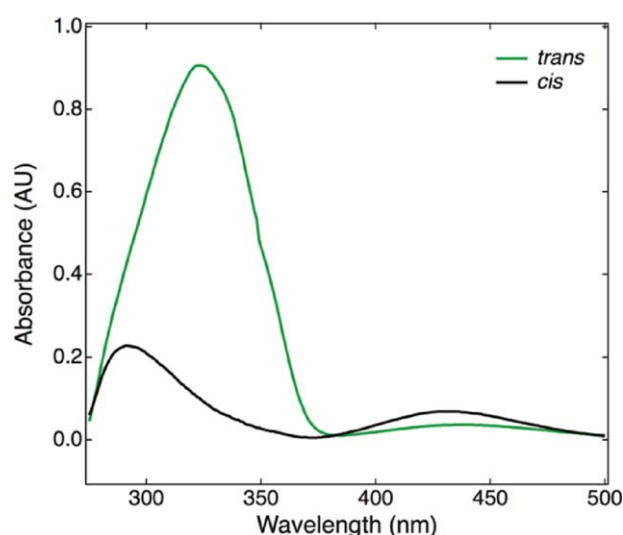


FIGURE 5 UV-vis spectrum for fully *trans* (green) and fully *cis* (black) isomerized AzoMA in BsA (28-17) at 0.02 wt% in BMI TFSI. [Color figure can be viewed at wileyonlinelibrary.com]

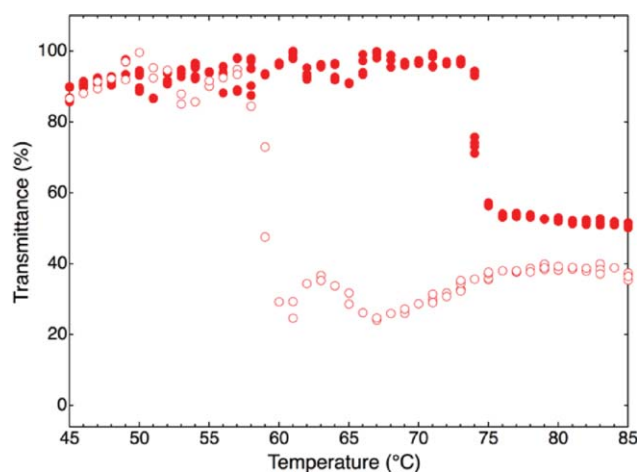


FIGURE 6 Representative cloud points of 10 wt% BsA (35-6) in EMI TFSI under UV (closed symbols) and visible light (open symbols) at a thickness of 100 μm . [Color figure can be viewed at wileyonlinelibrary.com]

a substantial dependence on sample thickness, as expected. For both 1500 and 500 μm , the UV cloud points occur at approximately the same temperature as under visible light. For these samples, the surface layer that is isomerized by the UV light before it is absorbed is small in comparison to the bulk. Once the visible light phase transition temperature is reached, the bulk will become turbid, giving the same cloud point as under visible light. As the samples become thinner, the visible and UV light phase separation temperatures diverge, as the sample thickness approaches the penetration depth of the UV light. Increasing the window between the two cloud points allows for more reliable light-triggered phase separation—minor temperature fluctuations, such as increased heat from turning on a UV lamp, will not change the temperature enough to move outside of the window. Notably, the difference between the UV and visible light phase separation temperatures do not reach a plateau. This suggests that the penetration depth is still < 25 μm for these samples. Due to signal limitations, this reflection setup was not able to measure below 25 μm . A penetration depth can be estimated based on the extinction coefficient obtained from UV-vis spectrophotometry. This can be done at 324 nm, the peak of absorbance in the UV region, as well as at 365 nm, the peak output of the UV lamp utilized. The output of the UV lamp is centered at 365 nm; however, the filter does not fully cut out shorter wavelength UV light, thus the true penetration depth likely falls between these two. For both wavelengths, the extinction coefficient depends on the isomerization state of the AzoMA, where the *trans* isomer has a higher absorptivity than the *cis*. As the surface is exposed to UV light, the isomerization of the surface to *cis* will increase the penetration depth. Therefore, the estimated penetration depth is expressed as a range for each polymer. For BsA (17-6), the penetration depth for a 10 wt% solution in EMI TFSI was estimated as 10–90 μm at 324 nm and 80–600 μm at 365 nm (calculation discussed in Supporting Information). As the azobenzene content is constant for all molecular weights, the penetration depths for all three polymers with 6 mol% AzoMA incorporation should be the

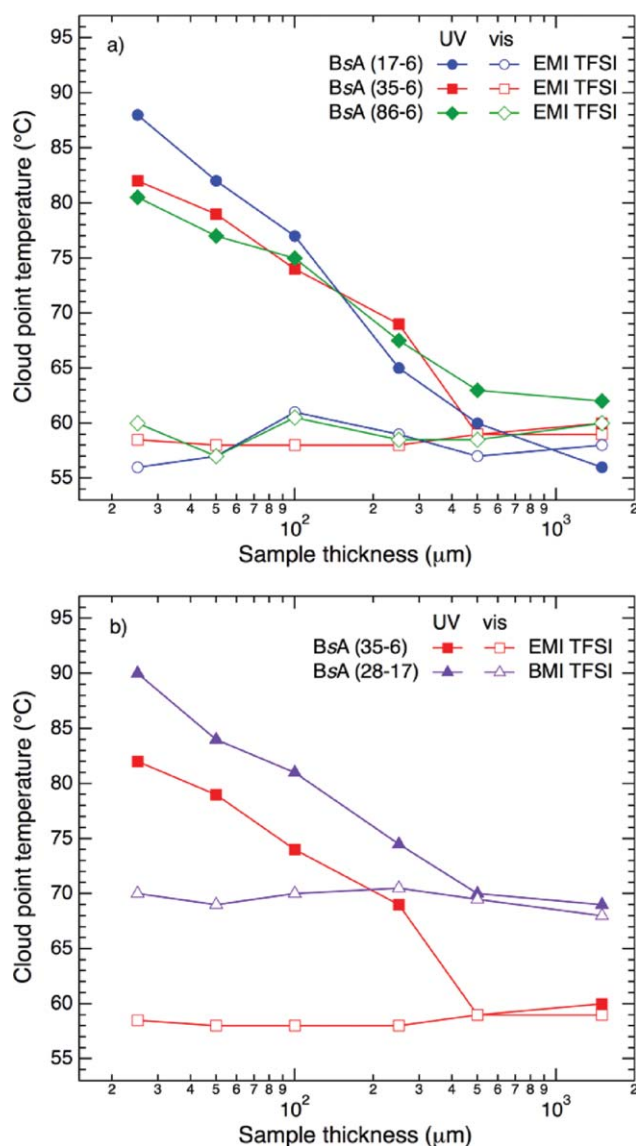


FIGURE 7 Cloud point temperatures of (a) varying molecular weights of 10 wt% P(BzMA-*stat*-(6 mol%)AzoMA) in EMI TFSI and (b) varying AzoMA content in 10 wt% P(BzMA-*stat*-AzoMA) in EMI/BMI TFSI under UV and visible light as a function of sample thickness. [Color figure can be viewed at wileyonlinelibrary.com]

same. Given these ranges, it is not unreasonable to assume that the samples are still thicker than the penetration depth of UV light. There is possibly a minor molecular weight dependence for the two thinnest samples, where the lowest molecular weight has the widest temperature window between UV and visible light phase separation. This may be a result of higher chain mobility, allowing some of the isomerized AzoMA chains under UV light near the surface to move further in the sample, giving a higher phase separation temperature under UV light only. There is minimal difference for the other two molecular weights, or for samples thicker than 100 μm. In general, therefore, the data are consistent with the conclusion that the cloud points are independent of molecular weight. This follows expectation for polymer/solvent systems that have LCST phase

behavior such as PNIPAm in water, which has an LCST of *ca.* 32 °C across a range of molecular weights.²⁸

The effects of increasing the AzoMA content in the copolymer did not follow the expected trend. In a range of compositions of P(NIPAm-*stat*-AzoMA) copolymers in ionic liquid, it was previously found that increasing the AzoMA content increased the window between the phase separation temperatures under UV and visible light.²² In contrast, Figure 7(b) shows that the window is virtually the same. In increasing the AzoMA content, it is expected that a larger polarity change will be induced in the polymer sample. This larger change in polarity should lead to a bigger difference between the visible and UV light phase separation temperatures. However, increasing the AzoMA content also increases the absorbance of UV light, decreasing the penetration depth in the sample. The penetration depth for a 10 wt% solution of BsA (28-17) in BMI TFSI was estimated as 4–40 μm at 324 nm and 30–450 μm at 365 nm. This is significantly reduced from the penetration depths for the 6 mol% AzoMA incorporation polymers. As a result, the range of sample thicknesses accessible for the reflective cloud point measurements are further from reaching full penetration of UV light for BsA (28-17). If the samples were able to be tested at thicknesses equal to or less than the penetration depth of the UV light, BsA (28-17) would likely show the largest cloud point temperature window. The previous work on the BzMA/AzoMA copolymers used only EMI TFSI, and as such was unable to get copolymers with compositions higher than 4 mol% AzoMA to dissolve in the ionic liquid.²⁴ Additionally, heating rate may play an effect on the cloud point temperature window. Ref. 24 used a heating rate of 0.1 °C/min, an order of magnitude less than what was used for these tests. While the slower heating rate may allow for a more precise

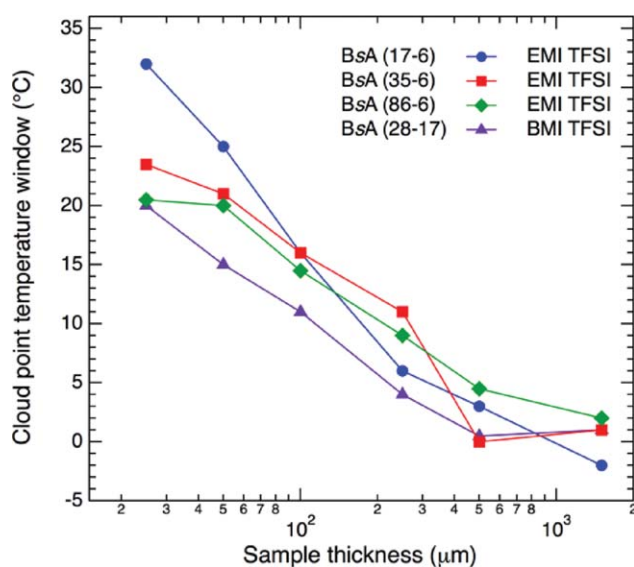


FIGURE 8 Temperature window between UV and visible light cloud point temperatures for the four polymers tested, across the range of sample thicknesses. [Color figure can be viewed at wileyonlinelibrary.com]

determination of the phase separation temperature, it also drastically increases the experiment time per sample.

The data for cloud point temperature windows are collected in Figure 8. All four polymers show a similar trend with respect to sample thickness, and all can achieve a bistable window of 20–30 °C. In general, BsA (28-17) shows the narrowest window, with BsA (35-6) and BsA (86-6) being very similar to each other and having a slightly broader window. These two polymers can both be compared with BsA (28-17) in different ways—BsA (35-6) has a similar molecular weight and BsA (86-6) has the same average number of AzoMA molecules per single polymer chain (Table 1). As the samples have not reached the thickness equal to or less than the penetration depth of UV light, we cannot state definitively which of these variables matters more. Finally, the smallest molecular weight chain BsA (17-6) shows the broadest temperature window for the two thinnest samples tested, potentially as a result of diffusional mixing.

CONCLUSIONS

A new method for readily varying the sample thickness in cloud point measurements was developed. This setup allowed for the screening of the phase separation behavior of four polymers under a range of six sample thicknesses, from 25 to 1500 μm . Studying the effect of sample thickness gives an idea of how thin the samples need to be to approach full penetration of UV light through the sample. This was not achieved for any of the samples, even at 25 μm , as evidenced by a continuing increase in the window between the phase separation temperatures under UV and visible light. However, even without full penetration of the UV light, windows as large as 20–30 °C were measured. This temperature difference is large enough to envision using poly(BzMA-*stat*-AzoMA) copolymers for further work in photo-responsive systems, such as light-induced micellization and gel network formation. The lack of molecular weight dependence in the phase separation temperature is also favorable for these applications. By knowing the phase separation temperature of a poly(BzMA-*stat*-AzoMA) copolymer at the concentration used, the bistable window for triggering micellization or gelation with light can be predicted. Target copolymer compositions can maintain low AzoMA content, and still have a broad temperature window for triggering as well. The less AzoMA that is necessary, the less “specialty” monomer needed. This also increases the likelihood that samples on the order of hundreds of nanometers thick will enable full penetration of UV light.

ACKNOWLEDGMENTS

This work was supported by the National Science Foundation through award DMR-1707578. The authors thank Prof. Jennifer

Laaser and Peter Schmidt for help putting together the home-built cloud point setup.

REFERENCES AND NOTES

- 1 B. A. Susan, H. Kaneko, T. Noda, A. M. Watanabe, *J. Am. Chem. Soc.* **2005**, *127*, 4976.
- 2 M. P. Scott, C. S. Brazel, M. G. Benton, J. W. Mays, D. Holbrey, R. D. Rogers, *Chem. Commun.* **2002**, 1370.
- 3 T. Welton, *Chem. Rev.* **1999**, *99*, 2071.
- 4 W. Lu, A. G. Fadeev, B. Qi, E. Smela, B. R. Mattes, J. Ding, G. M. Spinks, J. Mazurkiewicz, D. Zhou, G. G. Wallace, D. R. MacFarlane, S. A. Forsyth, M. Forsyth, *Science* **2002**, *297*, 983.
- 5 H. Yuan, H. Shimotani, A. Tsukazaki, A. Ohtomo, M. Kawasaki, Y. Iwasa, *Adv. Funct. Mater.* **2009**, *19*, 1046.
- 6 Q. Gan, D. Rooney, M. Xue, G. Thompson, Y. Zou, *J. Membr. Sci.* **2006**, *280*, 948.
- 7 Y.-Y. Jiang, Z. Zhou, Z. Jiao, L. Li, Y.-T. Wu, Z.-B. Zhang, *J. Phys. Chem. B* **2007**, *111*, 5058.
- 8 S. Liu, L. Zhou, P. Wang, F. Zhang, S. Yu, Z. Shao, B. Yi, *ACS Appl. Mater. Interfaces* **2014**, *6*, 3195.
- 9 Y. He, T. P. Lodge, *Chem. Commun.* **2007**, 2732.
- 10 S. So, R. Hayward, *ACS Appl. Mater. Interfaces* **2017**, *9*, 15785.
- 11 H. Asai, K. Fujii, T. Ueki, S. Sawamura, Y. Nakamura, Y. Kitazawa, M. Watanabe, Y.-S. Han, T.-H. Kim, M. Shibayama, *Macromolecules* **2013**, *46*, 1101.
- 12 T. Ueki, M. Watanabe, *Chem. Lett.* **2006**, *35*, 964.
- 13 K. Fujii, T. Ueki, K. Niitsuma, T. Matsunaga, M. Watanabe, M. Shibayama, *Polymer* **2011**, *52*, 1589.
- 14 T. Ueki, M. Watanabe, *Langmuir* **2007**, *23*, 988.
- 15 M. Matsugami, K. Fujii, T. Ueki, Y. Kitazawa, Y. Umebayashi, M. Watanabe, M. Shibayama, *Anal. Sci.* **2013**, *29*, 311.
- 16 Y. He, T. P. Lodge, *Macromolecules* **2008**, *41*, 167.
- 17 J. A. Syrett, C. R. Becer, D. M. Haddleton, *Polym. Chem.* **2010**, *1*, 978.
- 18 S. D. Bergman, F. Wudl, *J. Mater. Chem.* **2008**, *18*, 41.
- 19 T. Ueki, R. Usui, Y. Kitazawa, T. P. Lodge, M. Watanabe, *Macromolecules* **2015**, *48*, 5928.
- 20 G. S. Hartley, *Nature* **1937**, *140*, 281.
- 21 X. Ma, R. Usui, Y. Kitazawa, R. Tamate, H. Kokubo, M. Watanabe, *Macromolecules* **2017**, *50*, 6788.
- 22 T. Ueki, Y. Nakamura, A. Yamaguchi, K. Niitsuma, T. P. Lodge, M. Watanabe, *Macromolecules* **2011**, *44*, 6908.
- 23 T. Ueki, Y. Nakamura, T. P. Lodge, M. Watanabe, *Macromolecules* **2012**, *45*, 7566.
- 24 T. Ueki, A. Yamaguchi, N. Ito, K. Kodama, J. Sakamoto, K. Ueno, H. Kokubo, M. Watanabe, *Langmuir* **2009**, *25*, 8845.
- 25 T. Ueki, A. Yamaguchi, M. Watanabe, *Chem. Commun.* **2012**, *48*, 5133.
- 26 T. Fukuda, H. Matsuda, T. Shiraga, T. Kimura, M. Kato, N. K. Viswanathan, J. Kumar, S. K. Tripathy, *Macromolecules* **2000**, *33*, 4220.
- 27 S.-C. Tsao, C.-T. Lo, *RSC Adv.* **2014**, *4*, 23585.
- 28 M. Heskins, J. E. Guillet, *J. Macromol. Sci. A* **1968**, *2*, 1441.